

Two-Dimensional Moiré Polaronic Electron Crystals

Eric A. Arsenault^{1,*}, Yiliu Li^{1,*}, Birui Yang², Xi Wang^{3,4}, Heonjoon Park³, Edoardo Mosconi⁵, Enrico Ronca⁶, Takashi Taniguchi⁷, Kenji Watanabe⁸, Daniel Gamelin⁴, Andrew Millis², Cory R. Dean²

Filippo de Angelis^{5,6,9,10}, Xiaodong Xu^{3,11} and X. Y. Zhu^{1,†}

¹Department of Chemistry, Columbia University, New York, New York 10027, USA

²Department of Physics, Columbia University, New York, New York 10027, USA

³Department of Physics, University of Washington, Seattle, Washington 98195, USA

⁴Department of Chemistry, University of Washington, Seattle, Washington 98195, USA

⁵Istituto CNR di Scienze e Tecnologie Chimiche (CNR-SCITEC), CLHYO, 06123 Perugia, Italy

⁶Department of Chemistry, Biology and Biotechnology, University of Perugia, 06123, Perugia, Italy


⁷International Center for Materials Nanoarchitectonics, National Institute for Materials Science, Tsukuba, Ibaraki 305-0044, Japan

⁸Research Center for Functional Materials, National Institute for Materials Science, Tsukuba, Ibaraki 305-0044, Japan

⁹Department of Mechanical Engineering, Prince Mohammad Bin Fahd University, Al Khobar, 31952, Saudi Arabia

¹⁰SKKU Institute of Energy Science and Technology, Sungkyunkwan University, Suwon, Korea 440-746

¹¹Department of Materials Science and Engineering, University of Washington, Seattle, Washington 98195, USA

 (Received 18 September 2023; revised 3 February 2024; accepted 23 February 2024; published 20 March 2024)

Two-dimensional moiré materials have emerged as the most versatile platform for realizing quantum phases of electrons. Here, we explore the stability origins of correlated states in WSe₂/WS₂ moiré superlattices. We find that ultrafast electronic excitation leads to partial melting of the Mott states on timescales 5 times longer than predictions from the charge hopping integrals and that the melting rates are thermally activated, with activation energies of 18 ± 3 and 13 ± 2 meV for the one- and two-hole Mott states, respectively, suggesting significant electron-phonon coupling. A density functional theory calculation of the one-hole Mott state confirms polaron formation and yields a hole-polaron binding energy of 16 meV. These findings reveal a close interplay of electron-electron and electron-phonon interactions in stabilizing the polaronic Mott insulators at transition metal dichalcogenide moiré interfaces.

DOI: [10.1103/PhysRevLett.132.126501](https://doi.org/10.1103/PhysRevLett.132.126501)

Realizing quantum phases of electrons with high critical temperatures (T_c) has been one of the most important goals in quantum materials research, as exemplified by the longstanding and sometimes contentious quest for high T_c superconductors. Since the discoveries in magic-angle twisted bilayer graphene [1,2], moiré interfaces have become rich playgrounds for quantum phases. We focus on transition metal dichalcogenide (TMD) moiré superlattices that host a plethora of correlated charge orders [3–12]. The ordered phases are commonly observed at cryogenic temperatures, but a few exhibit high T_c , e.g., ~ 150 K for Mott states [4,5,8,10,12]. While mechanistic discussions have focused on many-body electron-electron (e-e) interactions, the potential role of electron-phonon (e-ph) interactions has been mostly neglected. In the related phenomena of charge density waves (CDWs) [13], e-e and e-ph interactions play equally important roles. Periodic modulation of electron density is accompanied by periodic lattice distortion in a CDW, as one introduces modulations in the potential landscape of the other. Here, we explore if periodic electron density in a moiré superlattice also introduces periodic lattice distortion from e-ph coupling.

For electrons excited out of an ordered state, the timescale for melting is dictated by that of the electron hopping integral (t), $\tau_e \sim \hbar/t$, or the period of the relevant phonon mode, τ_{ph} , when the ordering is dominated by e-e or e-ph interactions, respectively [14]. For TMD moiré superlattices hosting correlated states, the hopping integrals are $t \sim 1\text{--}5$ meV [3,15], corresponding to $\tau_e \sim 660\text{--}130$ fs. If e-ph coupling is important, the localization of an electron or hole to a moiré unit cell can be considered as a small polaron [16,17]. Deformation of the moiré unit cell likely involves acoustic phonons [16] in the momentum range defined by the moiré mini-Brillouin zone, with mean frequencies in the range of $\sim 0.1\text{--}1$ THz [18] or timescales of $\sim 10\text{--}1$ ps.

Correlated insulator states and exciton sensing.— We choose WSe₂/WS₂ heterobilayers with twist angles $\theta = 0 \pm 1^\circ$ and $60 \pm 1^\circ$, where correlated electronic states have been demonstrated with exciton sensing [4,5,8,10]. The moiré lattice constants ($a_M \sim 8$ nm) are the same and band flattening occurs at both twist angles, leading to the observation of similar correlated electronic states. Figure 1(a) shows the device structure, with an optical

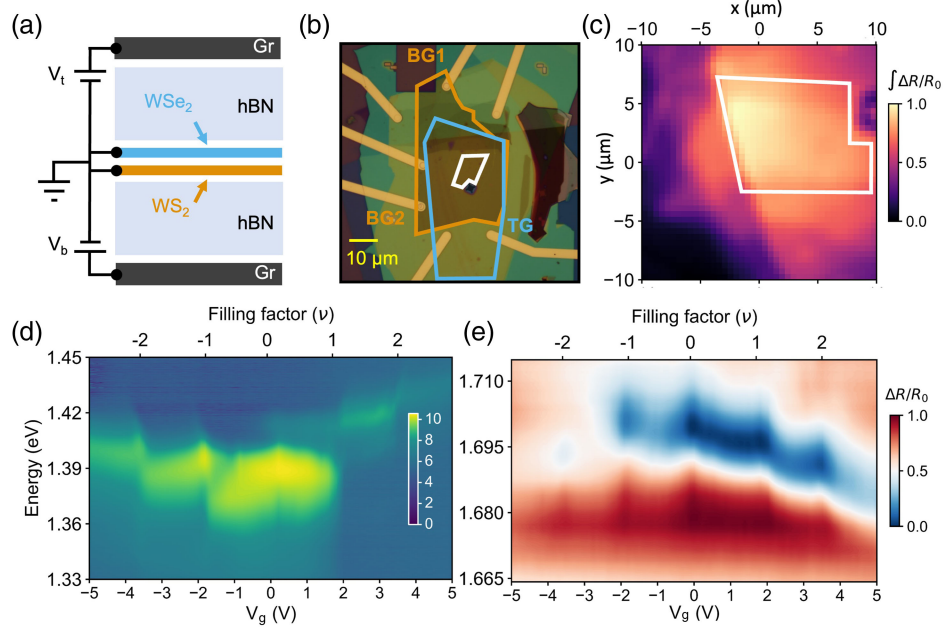


FIG. 1. WSe_2/WS_2 device ($\theta = 60^\circ$, D1): structure and characterization. (a) Schematic of the device showing the top (V_t) and bottom (V_b) gates consisting of few-layer graphite (Gr) and hexagonal boron nitride (hBN) encapsulating the WSe_2/WS_2 heterobilayer. (b) Optical image of the sample where the top and bottom gates are labeled, along with outlines showing the Gr electrodes (blue and orange lines corresponding to the top and bottom electrodes, respectively) and the WSe_2/WS_2 overlap region (white line). (c) Steady-state reflectance contrast mapping with the white line highlighting the WSe_2/WS_2 overlap region. $\Delta R = R - R_0$; R is the reflectance from the sample in the bilayer region and R_0 is reflectance from the sample stack without the bilayer. (d) Gated ($V_g = V_t = V_b$) steady-state photoluminescence spectrum (with intensity shown on a logarithmic scale). (e) Gated ($V_g = V_t = V_b$) steady-state reflectance spectrum of the lowest energy moiré exciton of WSe_2 . All data collected at 11 K.

image of the 60° device (D1), Fig. 1(b), and the reflectance map, Fig. 1(c). Under negative (positive) gate bias (V_g), holes (electrons) are injected into the heterojunction and, due to type-II band alignment, reside in the WSe_2 (WS_2) layer [4,5]. We control the moiré lattice filling factor (ν) by V_g and maintain a zero electric field unless otherwise noted. Here, $\nu < 0$ and $\nu > 0$ correspond to hole and electron doping, respectively. Two additional 0° samples (D2 and D3) are shown in Figs. S1 and S2 [19].

The oscillator strength of the sensing exciton is enhanced upon correlated state formation—a result of the accompanying reduction in the effective dielectric constant (ϵ_{eff}) [4,5,8,10]. This is shown for D1 in the photoluminescence spectrum from interlayer excitons, Fig. 1(d), and reflectance spectrum from intralayer excitons, Fig. 1(e). Both spectra as functions of V_g identify the charge neutral ($\nu = 0$), one- and two-hole ($\nu = -1, -2$), and one- and two-electron ($\nu = 1, 2$) states [8,12]. Similar results are obtained for the 0° devices (Figs. S1 and S2). While the $\nu = -1$ state has been called a Mott [29] or a charge-transfer insulator [30], the $\nu = -2$ state is a Mott insulator of double occupation [31].

We apply time-resolved reflectance spectroscopy and focus on the correlated hole states, because sensing from the WSe_2 moiré exciton is most sensitive to holes residing in the same layer. A correlated hole Mott state can be

represented by gap opening near the top of the valence band, resulting in a lower Hubbard band (LHB, with holes) and an upper Hubbard band (UHB, without holes). We choose a pump photon energy (1.55 eV) below the optical gaps of WSe_2 and WS_2 to avoid long-lived interlayer excitons [32]. At this photon energy, a hole in the LHB can be excited deep into the valence band; the excited hole cools on ultrafast timescales to reach the UHB, Fig. 2(a). The e-h pair across the Hubbard gap, Fig. 2(b), is usually called a holon-doublon pair [13,14]. The subsequent disordering may lead to partial gap closing, Fig. 2(c), with accompanying increase in ϵ_{eff} . Figures 2(d)–2(f) show 2D plots of transient reflectance as a function V_g at selected delays from the 60° device; the signal is $\Delta R/R$, where ΔR is the pump-induced reflectance change and R is the reflectance without pump. The peaks in $\Delta R/R$ only appear around V_g values commensurate with $\nu = -1$ and -2 and vary with Δt . Similar results are obtained for the 0° samples (Figs. S1 and S2).

Melting dynamics of the correlated states.—Figure 3 contains pump-probe data for the $\nu = 0, -1$, and -2 states of the 60° sample. These measurements are carried out in a pump fluence regime where two photon absorption does not contribute (see Figs. S3 and S4). The only observed dynamics for $\nu = 0$ [Fig. 3(a)] correspond to low frequency phonons, which appear as delayed and periodic

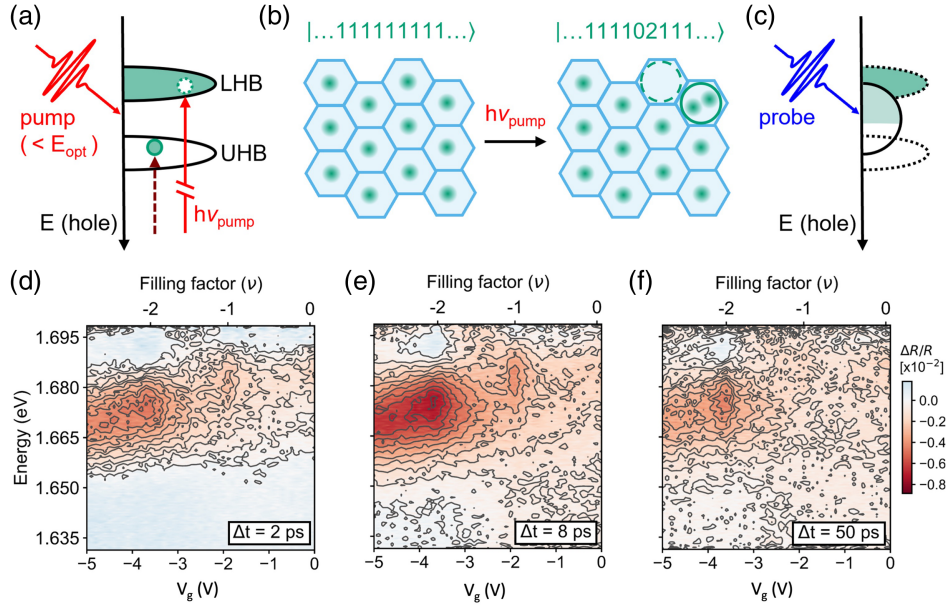


FIG. 2. Pump and probe of a hole Mott state in hole-doped WSe_2/WS_2 . (a) Excitation of a hole (green) from the lower Hubbard band (LHB) to a deep valence state, with subsequent cooling of the photoexcited hole (green sphere) to the upper Hubbard band (UHB). The hole energy scale is opposite to that of an electron scale. (b) Real space representation of the holon-doublon pair for the hole (green spheres) Mott state, with corresponding state representation on the top of each cartoon. (c) Partial melting (disordering) and gap closing from holon-doublon excitation. (d)–(f) Transient reflectance spectra plotted as a function of probe energy (covering the first moiré exciton of WSe_2) versus gate voltage ($V_g = V_t = V_b$) at $\Delta t = 2, 8, 50$ ps in (d)–(f), respectively. Features specific to the $\nu = -1, -2$ states can be observed and seen to evolve as a function of Δt . Here, $\Delta R/R$ is the transient reflectance signal calculated from pump-on and pump-off spectra. The pump fluence employed for the transient measurements was $57 \mu\text{J}/\text{cm}^2$. All spectra collected at 11 K.

modulations in $\Delta R/R$ on an otherwise flat background (see Figs. S5 and S6). For the $\nu = -1, -2$ states, in addition to phonons, we observe a decrease in overall $\Delta R/R$ in a few picoseconds, followed by recovery at longer times. The decrease in $\Delta R/R$ is attributed to an increase in ϵ_{eff} from disordering of the correlated states, which we refer to as “melting.” The melting times (τ_m) obtained from single exponential fits to the initial decays in $\Delta R/R$ in Figs. 3(b) and 3(c) (see Fig. S5 for details) are: $\tau_m = 3.2 \pm 0.2$ ps ($\nu = -1$) and 3.4 ± 0.1 ps ($\nu = -2$) at $T \leq 40$ K. These τ_m values are at least 5 times longer than those predicted from the charge hopping integrals, but are in the range estimated from acoustic phonons. The pump-induced changes to ϵ_{eff} are not resolved for fractional filling factors; see Fig. S7.

For either $\nu = -1$ or -2 , τ_m remains constant until ~ 40 K, above which it decays monotonically; see Fig. 4(a). There are two regions: (1) at $T \leq 40$ K, temperature independence is expected from predominantly e-e interactions; (2) at $T > 40$ K, e-ph interactions become important and melting is thermally activated. We plot melting rates, $k_m = 1/\tau_m$, with temperature, Figs. 4(b) and 4(c), for $\nu = -1, -2$, respectively, and fit the data to the Arrhenius equation, $k_m \propto \exp[-E_a/k_B T]$, where E_a is the activation energy and k_B the Boltzmann constant. A constant offset is included to account for the temperature-independent

contribution. These fits yield $E_a = 18 \pm 3$ meV and 13 ± 2 meV for the $\nu = -1$ and -2 , respectively.

The activation energies obtained from melting rates are on the order of thermal dissociation energies estimated from T_c . While intensity of the sensing exciton in static reflectance (Fig. S8) may be used as a proxy to the order parameter in the Mott states [4,8], the presence of background signal makes analysis difficult. We use transient reflectance instead for $\nu = -1$ (green) and -2 (purple), with $\nu = 0$ (black) as a control; see Fig. 4(d). The correlated states are still observed at ~ 150 K and ~ 100 K for $\nu = -1, -2$, respectively, providing lower bounds for T_c . These give $k_B T_c \sim 13$ meV and ~ 9 meV for $\nu = -1$ and -2 , respectively; they are $\sim 70\%$ of the E_a values.

The temperature-dependent measurements are also repeated on a second 0° sample (D2) (Fig. S9). We obtain $\tau_m = 3.4 \pm 0.2$ ps for $\nu = -1$ at $T = 8$ K. The temperature dependence in τ_m at $T > 40$ K gives $E_a = 19 \pm 3$ meV and that of $\Delta R/R$ signal gives $T_c \sim 150$ K for the $\nu = -1$ state. These results are in excellent agreement with those measured in the 60° sample (D1) and confirm that the similar thermal dissociation temperatures observed for the correlated states in the 0° and 60° samples share the same physical origin. The differences in the moiré potential trap depth at 0° are 60° [33] do not seem to impact the melting or

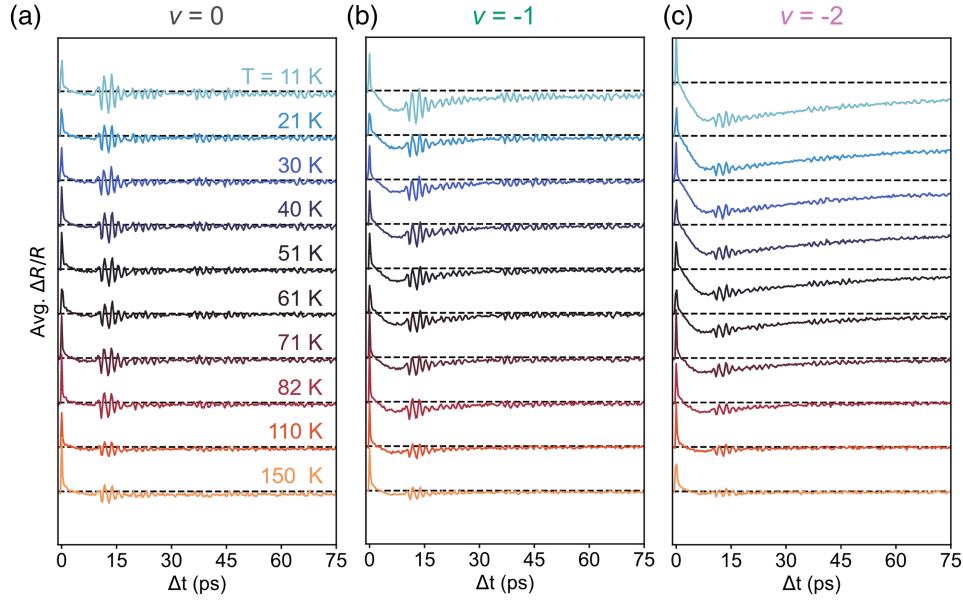


FIG. 3. Temperature-dependent temporal response of correlated states. (a)–(c) Transient reflectance traces of the $\nu = 0, -1, -2$ states, respectively, averaged over a ~ 0.01 eV probe energy range about the maximum of the lowest energy moiré band of WSe_2 . The coherent artifact resulting from pump-probe overlap can be seen at $\Delta t = 0$ ps. The time traces have been offset for clarity. The colors corresponding to each temperature are labeled in panel (a) and are consistent throughout the figure. The employed pump fluence was $14 \mu\text{J}/\text{cm}^2$. All data shown are for sample D1.

reordering dynamics of the Mott states. While we focus on melting, the recovery dynamics (Fig. S10) are more complex. The recovery of the $\nu = -1$ state is essentially temperature-independent, suggesting that e-e scattering limits the reformation of the Mott state [34]. The recovery of the $\nu = -2$ state, however, shows significant temperature dependence, pointing to the role of e-ph interactions. These processes deserve further investigations.

Polaronic nature of the correlated Mott insulators.—The melting rates and, more importantly, their thermal activations suggest electron-phonon coupling in the $\nu = -1$ and -2 Mott states. In a correlated insulator, the residence time of each electron (hole) in a moiré unit cell is much longer

than that of an uncorrelated electron, due to inhibition of charge hopping and much reduced kinetic energy in the former. The long residence time can lead to local polarization of the lattice to form a small polaron with the signature thermal activation [16]. The correlated insulator states are likely small polaron lattices. Here, we use “small” to describe the size of the polaron with respect to the moiré length scale.

To corroborate polaron formation, we carry out density functional theory (DFT) calculations based on the Perdew-Burke-Ernzerhof (PBE) exchange-correlation functional on a $\theta = 0^\circ$ WSe_2/WS_2 bilayer (Supplemental Material, Fig. S11). We first relax the structure of the neutral system,

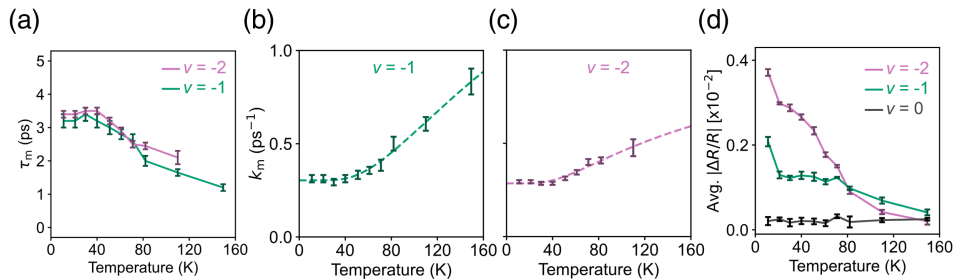


FIG. 4. Polaronic nature of correlated states. (a) Temperature-dependent melting time (τ_m) of the $\nu = -1, -2$ states resulting from the pump pulse. (b),(c) Melting rates, k_m , corresponding to panel (a). The dashed lines are fits to the Arrhenius equation to extract thermal activation energies for $\nu = -1, -2$ of $E_a = 18 \pm 3$ meV and 13 ± 2 meV, respectively. Constant offsets account for nonzero melting rates at lower temperatures. (d) Temperature-dependent transient reflectance for the $\nu = 0, -1, -2$ states (shown in gray, green, purple, respectively). For each data point, the corresponding transient reflectance spectra was averaged over a ~ 0.01 eV probe energy range about the maximum of the lowest energy WSe_2 moiré exciton peak and averaged over a pump-probe delay of $\Delta t = 4-8$ ps. All error bars indicate 99% confidence intervals. All data shown are for sample D1.

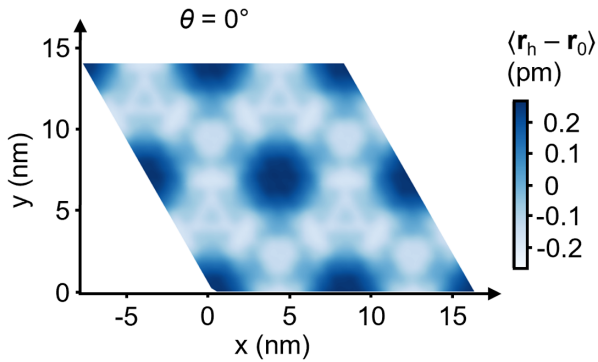


FIG. 5. *Ab initio* charge-induced lattice distortion. Structural reorganization averaged over the atomic positions on each lattice point upon injection of a positive charge in an aligned WS_2/WSe_2 bilayer. The color scale represents the degree of distortion at each lattice position, $\langle \mathbf{r}_h - \mathbf{r}_0 \rangle$.

followed by additional structural relaxation upon introducing a positive charge into the moiré unit cell ($v = -1$). Charge localization is evident from the spatial distribution of geometrical rearrangement, which occurs upon injection of a positive charge into each unit cell; see Fig. 5. The periodic electron density in the moiré superlattice introduces periodic lattice distortion, which is 90% perpendicular to the bilayer plane. We calculate a total reorganization energy of 16 meV; this can be taken as the polaron binding energy. This calculation is at the single-hole level, without the explicit inclusion of many-body correlations as captured by the Hubbard Hamiltonian [3]. The resulting polaron binding energy agrees surprisingly well with experimental activation energies; although PBE DFT is not expected to quantitatively account for e-ph coupling, it correctly describes the pattern of structural reorganization [35]. The disordering or melting of an ordered hole lattice requires hole hopping among moiré unit cells. In the small polaron picture, charge hopping requires thermal activation of phonons to overcome the polaron binding energy and release the hole from the trap. Thus, the thermal activation energy is related to the polaron binding energy [16,17,36].

Concluding comments.—The results presented here reveal the polaronic nature of correlated insulator states in the WSe_2/WS_2 moiré system. Our findings challenge the conventional many-body electron Hamiltonian and suggest the necessity of including e-ph coupling in some cases. In 2D materials, Kang *et al.* provided experimental evidence for Holstein “small” polaron formation in electron doped MoS_2 from intervalley coupling by zone-boundary longitudinal acoustic phonons [37]. Theoretically, Sio and Giustino reported polaron formation in h-BN; however, these authors suggested that Fröhlich “large” polaron formation from long-range Coulomb interaction is insignificant in 2D TMDs [38]. Recent theoretical work has also begun to explore e-ph coupling [39–41] in magic-angle

twisted bilayer graphene. As a final comment, the small polaron lattice that we report here for Mott states in the TMD moiré system is similar to a CDW state and e-ph interactions may be partially responsible for overall thermal stability.

X.-Y.Z. acknowledges support by DOE-BES under Award No. DE-SC0024343. C. R. D. acknowledges support for sample fabrication by the Materials Science and Engineering Research Center (MRSEC) through NSF Grant No. DMR-2011738. X. D. X. acknowledges support for sample preparation and characterization as part of Programmable Quantum Materials, an Energy Frontier Research Center funded by the U.S. Department of Energy (DOE), Office of Science, Basic Energy Sciences (BES), under Award No. DE-SC0019443. K. W. and T. T. acknowledge support from the JSPS KAKENHI (Grants No. 19H05790, No. 20H00354, and No. 21H05233). E. A. A. gratefully acknowledges support from the Simons Foundation as a Junior Fellow in the Simons Society of Fellows (965526). E. R. acknowledges funding from the European Research Council (ERC) under the Horizon Europe Research and Innovation Program (Grant No. ERC-StG-2021-101040197—QED-Spin). We thank Di Xiao, Ting Cao, Liang Fu, Shiwei Zhang, Jordan Pack, Yinjie Guo for valuable help and discussions. [20–28].

*These authors contributed equally to this work.

†Corresponding author: xyzhu@columbia.edu

- [1] Y. Cao *et al.*, Correlated insulator behaviour at half-filling in magic-angle graphene superlattices, *Nature (London)* **556**, 80 (2018).
- [2] Y. Cao, V. Fatemi, S. Fang, K. Watanabe, T. Taniguchi, E. Kaxiras, and P. Jarillo-Herrero, Unconventional superconductivity in magic-angle graphene superlattices, *Nature (London)* **556**, 43 (2018).
- [3] F. Wu, T. Lovorn, E. Tutuc, and A. H. Macdonald, Hubbard model physics in transition metal dichalcogenide moiré bands, *Phys. Rev. Lett.* **121**, 026402 (2018).
- [4] Y. Tang *et al.*, Simulation of Hubbard model physics in WSe_2/WS_2 moiré superlattices, *Nature (London)* **579**, 353 (2020).
- [5] E. C. Regan *et al.*, Mott and generalized Wigner crystal states in WSe_2/WS_2 moiré superlattices, *Nature (London)* **579**, 359 (2020).
- [6] L. Wang *et al.*, Correlated electronic phases in twisted bilayer transition metal dichalcogenides, *Nat. Mater.* **19**, 861 (2020).
- [7] Y. Shimazaki, I. Schwartz, K. Watanabe, T. Taniguchi, M. Kroner, and A. Imamoğlu, Strongly correlated electrons and hybrid excitons in a moiré heterostructure, *Nature (London)* **580**, 472 (2020).
- [8] Y. Xu, S. Liu, D. A. Rhodes, K. Watanabe, T. Taniguchi, J. Hone, V. Elser, K. F. Mak, and J. Shan, Correlated insulating states at fractional fillings of moiré superlattices, *Nature (London)* **587**, 214 (2020).

- [9] H. Li, S. Li, E. C. Regan, D. Wang, W. Zhao, S. Kahn, K. Yumigeta, M. Blei, T. Taniguchi, and K. Watanabe, Imaging two-dimensional generalized Wigner crystals, *Nature (London)* **597**, 650 (2021).
- [10] E. Liu, T. Taniguchi, K. Watanabe, N. M. Gabor, Y.-T. Cui, and C. H. Lui, Excitonic and valley-polarization signatures of fractional correlated electronic phases in a WSe_2/WS_2 moiré superlattice, *Phys. Rev. Lett.* **127**, 037402 (2021).
- [11] X. Wang, C. Xiao, H. Park, J. Zhu, C. Wang, T. Taniguchi, K. Watanabe, J. Yan, D. Xiao, and D. R. Gamelin, Light-induced ferromagnetism in moiré superlattices, *Nature (London)* **604**, 468 (2022).
- [12] X. Huang, T. Wang, S. Miao, C. Wang, Z. Li, Z. Lian, T. Taniguchi, K. Watanabe, S. Okamoto, and D. Xiao, Correlated insulating states at fractional fillings of the WS_2/WSe_2 moiré lattice, *Nat. Phys.* **17**, 715 (2021).
- [13] K. Rossnagel, On the origin of charge-density waves in select layered transition-metal dichalcogenides, *J. Phys. Condens. Matter* **23**, 213001 (2011).
- [14] S. Hellmann *et al.*, Time-domain classification of charge-density-wave insulators, *Nat. Commun.* **3**, 1069 (2012).
- [15] K. F. Mak and J. Shan, Semiconductor moiré materials, *Nat. Nanotechnol.* **17**, 1 (2022).
- [16] D. Emin, *Polarons* (Cambridge University Press, Cambridge, England, 2013).
- [17] C. Franchini, M. Reticcioli, M. Setvin, and U. Diebold, Polarons in materials, *Nat. Rev. Mater.* **6**, 1 (2021).
- [18] N. Mounet, M. Gibertini, P. Schwaller, D. Campi, A. Merkys, A. Marrazzo, T. Sohler, I. E. Castelli, A. Cepellotti, and G. Pizzi, Two-dimensional materials from high-throughput computational exfoliation of experimentally known compounds, *Nat. Nanotechnol.* **13**, 246 (2018).
- [19] See Supplemental Material at <http://link.aps.org/supplemental/10.1103/PhysRevLett.132.126501> for additional results and analysis, which includes Refs. [20–28].
- [20] L. J. McGilly *et al.*, Visualization of moiré superlattices, *Nat. Nanotechnol.* **15**, 580 (2020).
- [21] M. R. Rosenberger, H.-J. Chuang, K. M. McCreary, A. T. Hanbicki, S. v Sivaram, and B. T. Jonker, Nano-“squeegee” for the creation of clean 2D material interfaces, *ACS Appl. Mater. Interfaces* **10**, 10379 (2018).
- [22] J. Wang, Q. Shi, E.-M. Shih, L. Zhou, W. Wu, K. Barmak, J. Hone, C. Dean, and X. Zhu, Diffusivity reveals three distinct phases of interlayer excitons in $\text{MoSe}_2/\text{WSe}_2$ heterobilayers, *Phys. Rev. Lett.* **126**, 106804 (2021).
- [23] J. Wang, J. Ardelean, Y. Bai, A. Steinhoff, M. Florian, F. Jahnke, X. Xu, M. Kira, J. Hone, and X.-Y. Zhu, Optical generation of high carrier densities in 2D semiconductor heterobilayers, *Sci. Adv.* **5**, eaax0145 (2019).
- [24] Y. J. Bae *et al.*, Exciton-coupled coherent magnons in a 2D semiconductor, *Nature (London)* **608**, 282 (2022).
- [25] J. Hutter, M. Iannuzzi, F. Schiffmann, and J. VandeVondele, Cp2k: Atomistic simulations of condensed matter systems, *Comput. Mol. Sci.* **4**, 15 (2014).
- [26] J. VandeVondele, M. Krack, F. Mohamed, M. Parrinello, T. Chassaing, and J. Hutter, Quickstep: Fast and accurate density functional calculations using a mixed gaussian and plane waves approach, *Comput. Phys. Commun.* **167**, 103 (2005).
- [27] J. P. Perdew, K. Burke, and M. Ernzerhof, Generalized gradient approximation made simple, *Phys. Rev. Lett.* **77**, 3865 (1996).
- [28] D. G. A. Smith, L. A. Burns, K. Patkowski, and C. D. Sherrill, Revised damping parameters for the D3 dispersion correction to density functional theory, *J. Phys. Chem. Lett.* **7**, 2197 (2016).
- [29] F. Wu, T. Lovorn, E. Tutuc, and A. H. MacDonald, Hubbard model physics in transition metal dichalcogenide moiré bands, *Phys. Rev. Lett.* **121**, 026402 (2018).
- [30] Y. Zhang, N. F. Q. Yuan, and L. Fu, Moiré quantum chemistry: charge transfer in transition metal dichalcogenide superlattices, *Phys. Rev. B* **102**, 201115(R) (2020).
- [31] H. Park *et al.*, Dipole ladders with large Hubbard interaction in a moiré exciton lattice, *Nat. Phys.* **19**, 1286 (2023).
- [32] P. Rivera, H. Yu, K. L. Seyler, N. P. Wilson, W. Yao, and X. Xu, Interlayer valley excitons in heterobilayers of transition metal dichalcogenides, *Nat. Nanotechnol.* **13**, 1004 (2018).
- [33] L. Yuan, B. Zheng, J. Kunstmann, T. Brumme, A. B. Kuc, C. Ma, S. Deng, D. Blach, A. Pan, and L. Huang, Twist-angle-dependent interlayer exciton diffusion in $\text{WS}_2\text{-WSe}_2$ heterobilayers, *Nat. Mater.* **19**, 617 (2020).
- [34] N. Strohmaier, D. Greif, R. Jördens, L. Tarruell, H. Moritz, T. Esslinger, R. Sensarma, D. Pekker, E. Altman, and E. Demler, Observation of elastic doublon decay in the Fermi-Hubbard model, *Phys. Rev. Lett.* **104**, 080401 (2010).
- [35] K. Miyata, D. Meggiolaro, M. T. Trinh, P. P. Joshi, E. Mosconi, S. C. Jones, F. De Angelis, and X.-Y. Zhu, Large polarons in lead halide perovskites, *Sci. Adv.* **3**, e1701217 (2017).
- [36] T. Holstein, Studies of polaron motion: Part II. The “small” polaron, *Ann. Phys. (N.Y.)* **8**, 343 (1959).
- [37] M. G. Kang, S. W. Jung, W. J. Shin, Y. Sohn, S. H. Ryu, T. K. Kim, M. Hoesch, and K. S. Kim, Holstein polaron in a valley-degenerate two-dimensional semiconductor, *Nat. Mater.* **17**, 676 (2018).
- [38] W. H. Sio and F. Giustino, Polarons in two-dimensional atomic crystals, *Nat. Phys.* **19**, 629 (2023).
- [39] B. Lian, Z. Wang, and B. A. Bernevig, Twisted bilayer graphene: A phonon-driven superconductor, *Phys. Rev. Lett.* **122**, 257002 (2019).
- [40] Y. W. Choi and H. J. Choi, Dichotomy of electron-phonon coupling in graphene moiré flat bands, *Phys. Rev. Lett.* **127**, 167001 (2021).
- [41] M. Angeli, E. Tosatti, and M. Fabrizio, Valley Jahn-Teller effect in twisted bilayer graphene, *Phys. Rev. X* **9**, 041010 (2019).